Nucl Eng Technol 47 (2015) 567–578

Available online at www.sciencedirect.com

ScienceDirect

journal homepage: http://www.journals.elsevier.com/nuclear-engineering-and-technology/

Original Article

IMPROVEMENT OF CUPID CODE FOR SIMULATING FILMWISE STEAM CONDENSATION IN THE PRESENCE OF NONCONDENSABLE GASES

*JEHEE LEE, GOON-CHERL PARK, and HYOUNG KYU CHO**

Seoul National University, Department of Nuclear Engineering, Seoul, 151-742, South Korea

ARTICLE INFO

Article history:
Received 21 January 2015
Received in revised form
25 March 2015
Accepted 29 March 2015
Available online 16 June 2015

Keywords:
CUPID
Large system
Liquid film
Noncondensable gas
Wall condensation
Wall function

ABSTRACT

In a nuclear reactor containment, wall condensation forms with noncondensable gases and their accumulation near the condensate film leads to a significant reduction in heat transfer. In the framework of nuclear reactor safety, the film condensation in the presence of noncondensable gases is of high relevance with regards to safety concerns as it is closely associated with peak pressure predictions for containment integrity and the performance of components installed for containment cooling in accident conditions. In the present study, CUPID code, which has been developed by KAERI for the analysis of transient two-phase flows in nuclear reactor components, is improved for simulating film condensation in the presence of noncondensable gases. In order to evaluate the condensate heat transfer accurately in a large system using the two-fluid model, a mass diffusion model, a liquid film model, and a wall film condensation model were implemented into CUPID. For the condensation simulation, a wall function approach with a heat/mass transfer analogy was applied in order to save computational time without considerable refinement for the boundary layer. This paper presents the implemented wall film condensation model, and then introduces the simulation result using the improved CUPID for a conceptual condensation problem in a large system.

1. Introduction

The filmwise steam condensation on a wall plays an important role in the heat transfer processes in many industrial applications. However, when noncondensable gases are present during condensation, the heat transfer can be degraded significantly by the gases accumulating near the interface between the liquid film and the gas mixture [1]. In the framework of nuclear reactor safety, the film condensation in the presence of noncondensable gases is of high safety relevance since it is closely associated with peak pressure prediction in the containment and performance of components installed for the containment cooling in accident conditions, such as passive containment cooling systems. Therefore, a

* *Corresponding author.*
E-mail address: chohk@snu.ac.kr (H.K. Cho).

http://dx.doi.org/10.1016/j.net.2015.03.007
1738-5733/Copyright © 2015, Published by Elsevier Korea LLC on behalf of Korean Nuclear Society.

large number of experiments and analytical studies have been performed in order to investigate it and obtain accurate knowledge of condensation rates.

Up to now, lumped parameter simulation codes have been used for the prediction of thermal-hydraulic behaviors in containment buildings due to their large volume and long transient times which need to be simulated. Even though the lumped parameter codes cannot reproduce multidimensional phenomena adequately, acceptable estimates of heat transfer can be provided in reasonable computational time since those codes have been validated and improved against a vast experimental database. Recently, however, with increasing computing power, more and more researchers are resorting to computational fluid dynamics (CFD) in order to capture the details of multidimensional phenomena more accurately in nuclear applications, and hence overcome the drawbacks of the lumped parameter codes [2].

A comprehensive benchmarking activity using CFD codes for wall condensation was undertaken in the frame of SARNET [3], with the aim of setting up and developing models for steam condensation in conditions of interest for nuclear reactor containments. The benchmarking activity was performed against CONAN [4] experimental facility by various participants. Two different types of wall condensation models, in particular, the diffusion of vapor towards the interface, were tested: a local diffusion approach, which evaluates the mass flux using Fick's law approach; and the heat and mass transfer analogy, which uses the heat and mass transfer coefficient models. The former, sometimes referred to as a resolved boundary method [2], analyzes the wall film condensation with a considerable refinement of meshes close to the wall for an adequate evaluation of the mass fraction gradient of noncondensable gas. The latter, also known as a wall function method [2], does not require the refined discretization close to the wall, but the application can be limited to the conditions where the wall function is valid. In the SARNET benchmark, generally satisfactory prediction results were obtained with the two approaches thanks to the simplicity of the addressed system configuration. Martín-Valdepeñas et al. [5] also tested four different wall film condensation models in the presence of noncondensable gases using CFX-4 (AEA Technology Plc., Harwell, UK), an experimental correlation approach with three different heat and mass transfer analogy approaches. Recently, Vyskocil et al. [6], Zschaeck et al. [7], and Dehbi et al. [1] analyzed wall condensation heat transfer and an air-steam mixture for containment application using commercial CFDs, ANSYS-CFX (ANSYS Inc., Canonsburg, PA, USA) and FLUENT (ANSYS Inc.). The local diffusion approach was applied and the performance of the condensation models was tested on various experimental databases, such as CONAN test [4], PANDA [8], Kuhn test [9], COPAIN [10], TOSQAN [11], and on experimental models devised by Uchida et al. [12], Tagami [13], Dehbi et al. [14], and so on. Dehbi [2] simulated wall film condensation in the presence of noncondensable gases using ANSYS FLUENT and investigated the effect of near-wall mesh resolution on CFD predictions. He found that the wall function approach can underpredict condensation rates at boundary layer onset but if the boundary layer is developed, its predictions are reasonable.

In these CFD analyses listed above, a single-phase flow approach was applied and the effects of the condensation process on the flow and species distribution in the mixture phase were considered via user defined mass and energy sink terms. A liquid film on a condensate wall was neglected and this assumption was justified based on the fact that the condensate film heat transfer coefficient is much larger than the convective counterpart when the noncondensable amounts are significant [15]. In this way, most of the CFD analyses for the wall film condensation have been performed with the single-phase flow approach and not much research has been carried out with two-phase flow approaches. Mimouni et al. [16,17] proposed a wall condensation model for NEPTUNE-CFD which incorporates the two-fluid model for its governing equations and the condensation rate was estimated using the heat and mass transfer analogy approach. The model was validated against experimental data provided by TOSQAN [11] and COPAIN [10]. Meanwhile, a commercial CFD code, STAR-CCM+ [18], provides the wall condensation simulation with a thin liquid film using the fluid-film model. In the model, separate governing equations for the liquid film enable simulation of the falling liquid film on a condensate wall. The heat and mass transfer of the condensation in the presence of noncondensable gases is evaluated using the local diffusion approach. These two wall condensation models showed the advantages of the two-phase flow approaches in taking into account the effect of liquid film velocity on the gas velocity near the wall and their better applicability to more general conditions.

In the present study, the wall film condensation model was implemented into a computational multi fluid dynamics code developed at KAERI, named CUPID [19], which uses the two-fluid model for the governing equations. The ultimate objective of the implementation is extending its capability to the condensation heat exchanger analysis of a passive containment cooling system. At first, since the current version of CUPID does not include species mass transfer terms by a diffusion process, which are of crucial importance for the estimation of the noncondensable gas mass fraction on the liquid film surface, they were added into the mass and energy equations of CUPID. After that, the wall film condensation model was proposed based on the two-phase flow approach. Considering the large computational domain of the realistic application of the model, the wall function approach was adopted for the model without requiring a very fine computational grid. In this paper, the added mass diffusion terms are described and the code-to-code verification result for the terms against a commercial CFD code, STAR-CCM+, is presented. Afterwards, the wall film condensation model implemented into CUPID is summarized. For the verification of the model, a conceptual problem in the Dehbi [2] study was selected which dealt with a film condensation in a large control volume and the comparison result with the results from literature are discussed in order to confirm the validity of the implemented model.

2. Implementation of mass diffusion model into CUPID

The CUPID code has been developed at KAERI for a transient, three-dimensional analysis of two-phase flows in light-water nuclear reactor components [19]. It can provide both a

component-scale and a CFD-scale simulation by using a porous medium or an open medium model for a two-phase flow, respectively. It is based on a transient two-fluid, three-field model for a two-phase flow. The two fluids are gas and liquid, and the three fields refer to gas, continuous liquid, and droplets. Relevant physical models have been developed to close the governing equations, such as interfacial transfer models and the equations of state. The CUPID code has been validated against a set of test problems consisting of standard conceptual problems and experimental data. Its governing equations, numerical methods, and physical models are presented in Jeong et al. [20] and recent advances in the CUPID code are summarized in Yoon et al. [21], including the parallelization, coupling with the nuclear reactor system analysis code for a multi-scale analysis, and its application for the steam generator analysis.

CUPID includes the mass conservation equation of the noncondensable gas so that the gas mixture of steam and a noncondensable gas can be handled. Nevertheless, it neglects the mass and energy transfer due to a species diffusion induced by the spatial gradient of their mass fractions. This limits its gas mixture simulation capability to a highly convective flow where the effect of the mass diffusion can be ignored. In the filmwise condensation simulation, however, the species mass diffusion plays an important role to estimate the noncondensable gas mass fraction in a computational cell. If condensation occurs, the noncondensable gas accumulates near the interface between the gas mixture and the liquid film. At the same time, the accumulated noncondensable gas can be diluted by the species mass diffusion. Therefore, the noncondensable gas mass fraction can be over-predicted without considering the mass diffusion because of the over-estimated accumulation. This certainly results in the under-estimation of the film condensation rate. For this reason, the mass diffusion of the gas species and subsequent energy transfer with the species transport were implemented in the CUPID code to extend its capability to the film condensation. The modified species mass conservation equation and the energy transport equation are given by:

$$\frac{\partial}{\partial t}\left(\alpha_g\rho_g m_n\right)+\nabla\cdot\left(\alpha_g\rho_g m_n\vec{U}_g\right)=\underline{\nabla\cdot\left(\alpha_g\rho_g D\nabla m_n\right)}, \tag{1}$$

$$\begin{aligned}\frac{\partial\left(\alpha_g\rho_g e_g\right)}{\partial t}+\nabla\cdot\left(\alpha_g\rho_g e_g\vec{U}_g\right)=&-P\frac{\partial\alpha_g}{\partial t}-P\nabla\cdot\left(\alpha_g\vec{U}_g\right)+\ddot{q}_g\\&+\nabla\left(\alpha_g\vec{q}_g\right)+\frac{P_s}{P}H_{ig}\left[T_s(P_s)-T_g\right]\\&+\Gamma_v h_g^*-\left(\frac{P-P_s}{P}\right)H_{fg}\left(T_g-T_l\right)\\&+\underline{\nabla\cdot\left[\alpha_g\rho_g D(h_n-h_v)\nabla m_n\right]},\end{aligned} \tag{2}$$

where m_n is the noncondensable gas mass fraction, h_n is the noncondensable gas enthalpy, h_v is the vapor enthalpy, and D is the effective diffusivity which is the sum of the molecular diffusivity [22] and turbulent diffusivity [23]. The two terms underlined were added for the film condensation simulation in the present work.

For the verification of the implemented mass diffusion model, a conceptual problem was analyzed and the calculation result was compared with STAR-CCM+ result. Fig. 1 gives the problem description and indicates the computational domains, initial, and boundary conditions. The two-dimensional channel has a 10 m width and a 24 m height, the same as Dehbi's [2] conceptual problem. Initially, the channel was filled with a steam-air mixture with 50% steam by mass. Then, a steam-air mixture was injected from the inlet with air mass fractions of 80% and 50% for the central region and the other regions, respectively. The inlet fluid velocity and temperature were 0.3 m/s and 405 K. On the outlet, a constant pressure boundary condition was imposed to 4.0 bars. The calculations were conducted with the standard k-ε turbulence model and the gravitational force was excluded focusing on the effect of the mass diffusion term; 24,000 (100×240) cells were used for the conceptual problem.

In total, three cases of calculations were carried out with CUPID: (1) without the mass diffusion term (Case-1); (2) with the mass diffusion term (Case-2); and (3) with mass diffusion and 10 times larger mass diffusivity than Case-2, in order to show its qualitative influence on the noncondensable gas mass fraction (Case-3). Fig. 2 shows the calculation results of the air mass fraction for the three cases. The gradual diffusion of the noncondensable gas in the lateral direction and the increase of the mass diffusion with the mass diffusivity can be simulated reasonably. For more quantitative verification of the applied terms, the calculation result of the second case was compared with the STAR-CCM+ calculation results in Fig. 3, and they showed a very good agreement with each other. Supported by these simulations of a conceptual problem, it was verified that the mass diffusion model had been implemented into CUPID appropriately.

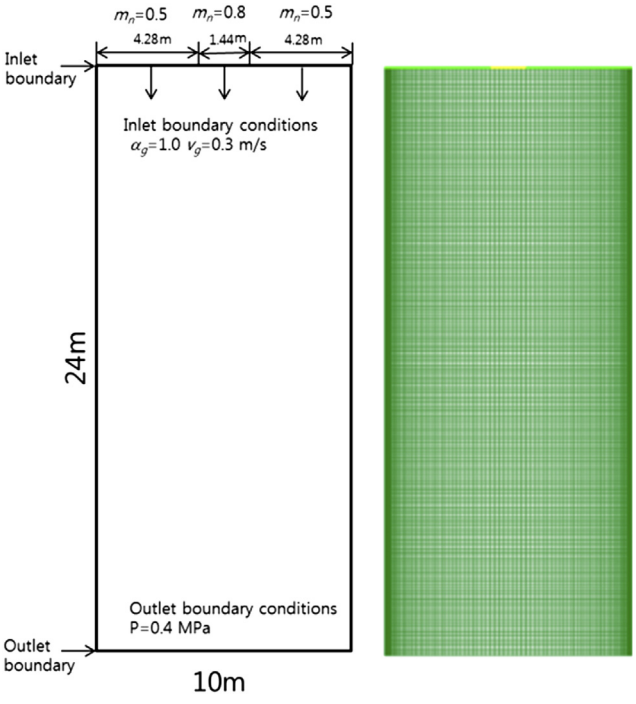

Fig. 1 – Conceptual problem for mass diffusion of a noncondensable gas.

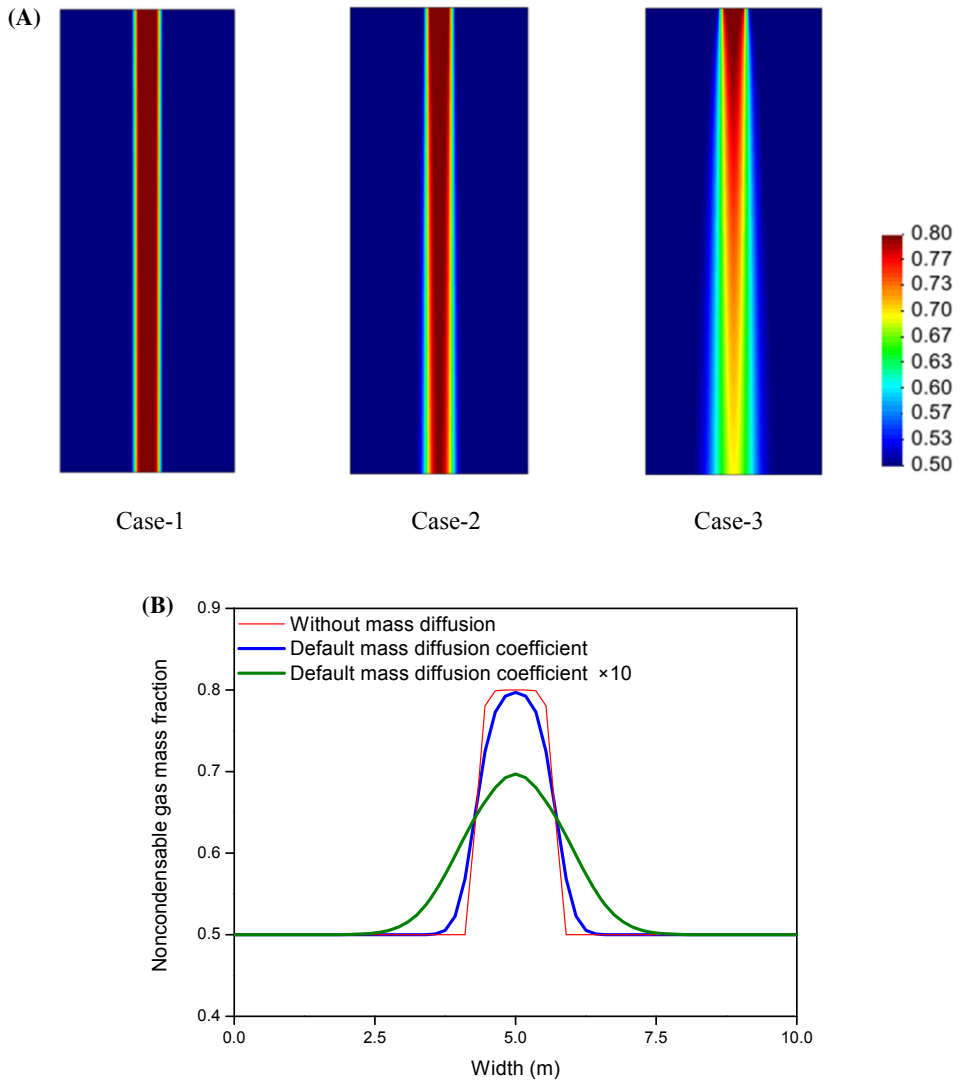

Fig. 2 – Calculation results: effect of mass diffusion term. (A) Noncondensable gas mass fraction. (B) Noncondensable gas mass fraction at the outlet.

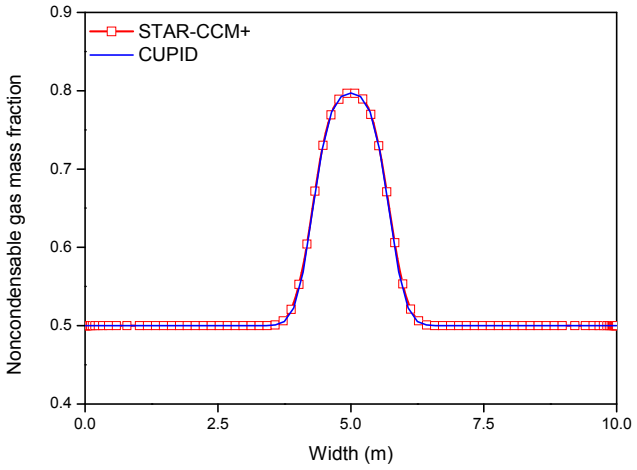

Fig. 3 – Code-to-code verification result: CUPID versus STAR-CCM+.

3. Implementation of film condensation model into CUPID

In the film condensation process, a thin liquid film is created on the condensate wall and it flows down along the wall. Generally, the thickness of the liquid film is too thin to resolve, so a subgrid liquid film model was implemented into CUPID in order to capture its behavior. CUPID gives the liquid film mass flow rate (Γ_f), the pressure drop, and the gas velocity in the wall adjacent cells to the liquid film model, then solves a momentum equation for the liquid film with the given mass flow rate and evaluates the wall and interfacial shear stresses. The evaluated stresses are transferred to CUPID and employed in the momentum equations of the two-fluid model. This exchange of information between CUPID and the liquid film model is repeated for all wall cells at every time step. The liquid film model is presented by Ghiaasiaan [24] with a fully

developed liquid film assumption. The momentum equation of a liquid film is:

$$\frac{d}{dy}\left[(\upsilon_l + E)\frac{dU_l}{dy}\right] - \frac{1}{\rho_l}\frac{dP}{dz} + g\sin\theta = 0, \quad (3)$$

where E is the eddy diffusivity in the liquid film and the correlation of Mudawar and El-Marsi [26] was applied to it. For boundary conditions, $U_l = 0$ at the wall and $dU_l/dy = \tau_i/\mu_l$ at the interface were imposed. The interfacial shear stress is expressed as:

$$\tau_i = \dot{f}\frac{1}{2}\rho_g|U_g - U_i|(U_g - U_i), \quad (4)$$

where $\dot{f}$ is the interfacial friction factor which makes the interfacial shear stress identical to the gas side shear stress evaluated by the law of the wall [25]. The nondimensionalized form of Eq. (3) can be numerically integrated if a mass flow (Γ_f) is given and the liquid film thickness (δ_f) is guessed. The velocity profile can then be obtained. For the numerical integration, 16 computational nodes were used across the liquid film thickness. The velocity profile is integrated to check the satisfaction of Eq. (5) and if it is not satisfied, the guessed liquid film thickness is modified until the convergence is achieved, as shown in Fig. 4.

$$\Gamma_f/\mu_l = \int_0^{\delta_f^*} U_l^* dy^*, \quad (5)$$

Where $U_l^* = U_l \Big/ \sqrt{\delta_f\left[-\frac{1}{\rho_l}\frac{dP}{dz} + g\sin\theta\right]}$,

$$\delta_f^* = \frac{\delta_f}{\upsilon_l}\sqrt{\delta_f\left[-\frac{1}{\rho_l}\frac{dP}{dz} + g\sin\theta\right]},$$

$$y^* = \frac{y}{\upsilon_l}\sqrt{\delta_f\left[-\frac{1}{\rho_l}\frac{dP}{dz} + g\sin\theta\right]}$$

Once the liquid film thickness and velocity profile are obtained, the wall shear stress of the liquid and the interfacial shear stress can be evaluated and used in CUPID's two-fluid model momentum equations.

In order to verify the implemented liquid film model in CUPID, a conceptual problem for a downward liquid film as shown in Fig. 5, was simulated. The conceptual problem is the simulation of the downward liquid film flow over a hypothetical vertical wall which is 2 m long. The channel width is 0.25 m and water is assumed to enter the channel from the top with a 0.12 kg/ms mass flow rate. The CUPID calculation results were compared with the analytical solution obtained from Eqs. (3) and (5) and the STAR-CCM+ simulation results. The liquid film thickness of CUPID was calculated from the liquid volume fraction and the width of the first cell from the wall. In the STAR-CCM+ calculation, the fluid-film model [18], which is devoted to thin film simulation, was applied. As shown in Fig. 6, the predicted downward liquid velocities in the wall adjacent cells were markedly decreased by the implementation of the wall shear stress model. Without it, the wall shear stress is under-estimated because the velocity gradient across the thin liquid film cannot be taken into account which results in significantly over-predicted liquid velocity. With the implemented model, the predicted liquid velocity and the film thickness are in reasonably good agreement with the analytical solution after being fully-developed and the STAR-CCM+ calculation results as presented in

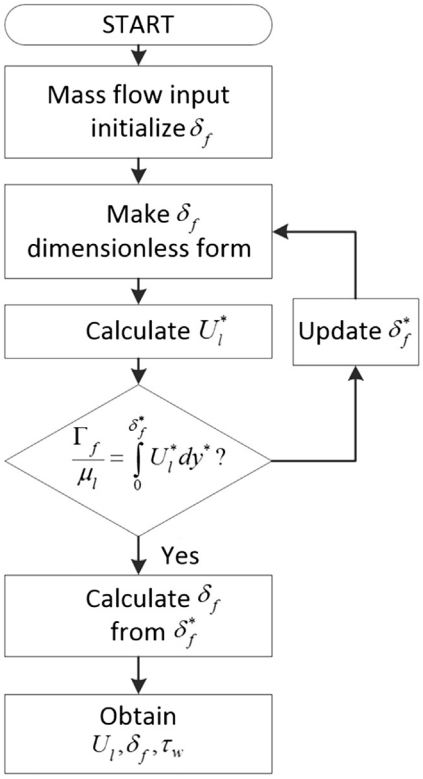

Fig. 4 – Flowchart of the liquid film model.

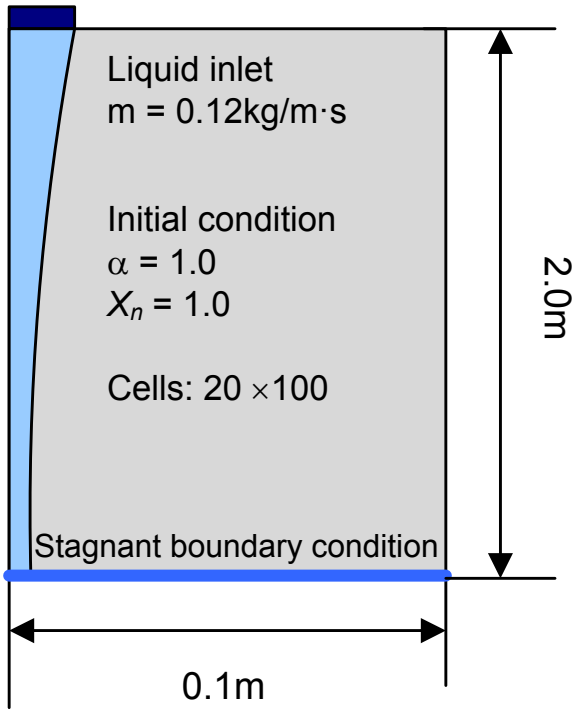

Fig. 5 – Conceptual problem for liquid film model.

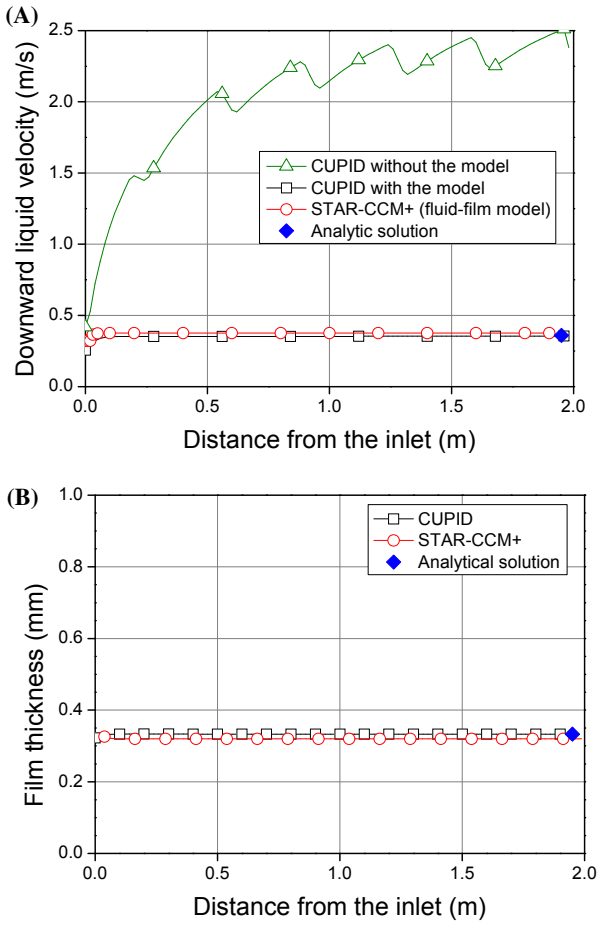

Fig. 6 – Calculation result for the liquid film model. (A) Downward liquid film velocity and thickness. (B) Liquid film thickness.

Fig. 6. The error between the analytical solution and the simulation result was < 2%.

A wall film condensation model was implemented into CUPID after the implementation of the liquid film model, which combines the models proposed by Ghiaasiaan [24] and Naylor and Friedman [27]. The following are the equations for the wall film condensation model.

– The interface temperature

$$T_i = T_s(X_{v,i}P), \tag{6}$$

where T_i represents interface temperature and $X_{v,i}$ is a vapor mole fraction at the interface. As shown in Fig. 7, mole fraction of steam decreases relatively at the interface because of noncondensable gas accumulation near the condensation wall. Therefore, the mole fraction of the interface should be estimated using bulk stream data transferred from CUPID. The flow properties and variables at $y^+ = 250$ were selected for the bulk stream values. This selection of the bulk properties was devised from the methodology determining mean-flow liquid temperature in boiling heat transfer simulations [28–30].

– Mass fraction at the interface

$$m_{v,i} = \frac{X_{v,i}M_v}{X_{v,i}M_v + (1 - X_{v,i})M_n}, \tag{7}$$

where M_v and M_n represent molecular weights of vapor and noncondensable gas, respectively.

– Condensation mass flux.

The condensation mass flux is evaluated with and without suction correction factors as below,

$$\begin{aligned} m'' &= -K_{g,i}B \text{ without suction correction,} \\ m'' &= -K_{g,i}B\theta_b \text{ with Bird's suction correction factor } (\theta_b), \\ m'' &= -K_{g,i}B\theta_c \text{ with Dehbi's suction correction factor } (\theta_c), \end{aligned} \tag{8}$$

where $K_{g,i}$ is the mass transfer coefficient, $B = \left(\frac{m_{v,i} - m_{v,b}}{1 - m_{v,i}}\right)$, $\theta_b = \frac{\ln(1+B)}{B}$, and $\theta_c = \frac{1}{2}(1 + \theta_b)$. Since there is a disagreement about the widely used Bird approach for its over-estimation of the condensation rate [1], two suction correction factors were applied to investigate their effect. The mass transfer coefficient was obtained from the wall function approach introduced in Martín-Valdepeñas et al. [5] based on the heat and mass transfer analogy as below.

$$K_{g,i} = H_{g,i}\left(\frac{\rho_g D_g}{k_g}\right)\left(\frac{Sc}{Pr}\right)^{1/3} \tag{9}$$

In this equation, the mass transfer coefficient ($K_{g,i}$) was evaluated from the convection heat transfer coefficient ($H_{g,i}$), calculated using the wall law.

– Heat balance equation

$$H_{g,i}(T_g - T_i) - \frac{k_f}{\delta_f}(T_i - T_w) + m''h_{fg} = 0, \tag{10}$$

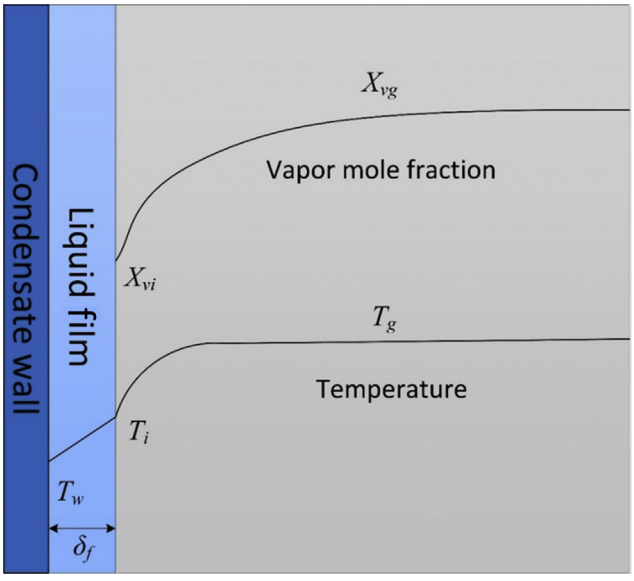

Fig. 7 – Vapor mole fraction near the condensation wall.

where, δ_f is the liquid film thickness from the film thickness model and the liquid-side heat transfer rate was obtained with the assumption that the temperature profile of the liquid film is linear.

A solution procedure is shown in Fig. 8 and the primary unknown in Eqs. (6)–(10) is vapor mole fraction at the interface. For the calculation, the mole fraction at the interface ($X_{v,i}$) is assumed at first, and interface temperature (T_i) and mass fraction of vapor ($m_{v,i}$) are calculated using the mole fraction. Thereafter, the condensation mass flux (m'') at the gas/liquid interface was calculated using Eq. (8). Total mass flow rate of a liquid film can then be obtained from the sum of the condensation mass flow rate and the convective mass flow rate from the upstream cell. When the total mass flow rate is determined, the film thickness can be calculated from the liquid film model. With the calculated film thickness, the interfacial heat transfer coefficient, and the condensation mass flux, the satisfaction of the heat balance equation at the interface, Eq. (10), is evaluated. By an iterative solution method, the solutions of Eqs. (6)–(10) can be obtained and the calculation proceeds to the next cell.

In a bid to connect this wall film condensation model described above with CUPID, the following terms in the governing equations of the two-fluid model were modified: wall shear stress; wall heat transfer; interfacial area concentration; interfacial shear stress; and interfacial heat transfer coefficients for gas and liquid.

In the original version of CUPID, the wall shear stress was evaluated by assuming that the portions of the two phases that cover the wall for the momentum exchange are determined from the volume fractions of each phase, and hence the wall shear stresses for each phase are weighted with them as shown below,

$$\dot{M}_{k,wall} = \nabla\cdot[\alpha_k(\mu_k\nabla U_k)], \tag{11}$$

where, k is gas or liquid. If the wall condensation model is activated, however, the wall is not covered by gas mixture but solely by liquid and the momentum exchange between the wall and a fluid should be considered for the liquid phase only. To this end, the wall shear stress terms for two phases were modified at first,

$$\dot{M}_{g,wall} = 0, \quad \text{and} \quad \dot{M}_{l,wall} = \nabla\cdot[(\mu_l\nabla U_l)]. \tag{12}$$

In addition to this, the wall shear stress is associated with the velocity gradient in a liquid film obtained from the liquid film model as follows,

$$\mu_l\nabla U_l = \mu_l\frac{U_{l,1} - U_{l,0}}{\delta y}, \tag{13}$$

where $U_{l,0}$ and $U_{l,1}$ are the wall velocity and the liquid velocity at the first node from the wall in the liquid film subgrid, respectively. With these modifications, the implemented liquid film model explicitly imposes the wall shear stress to the momentum equations of the two-fluid model.

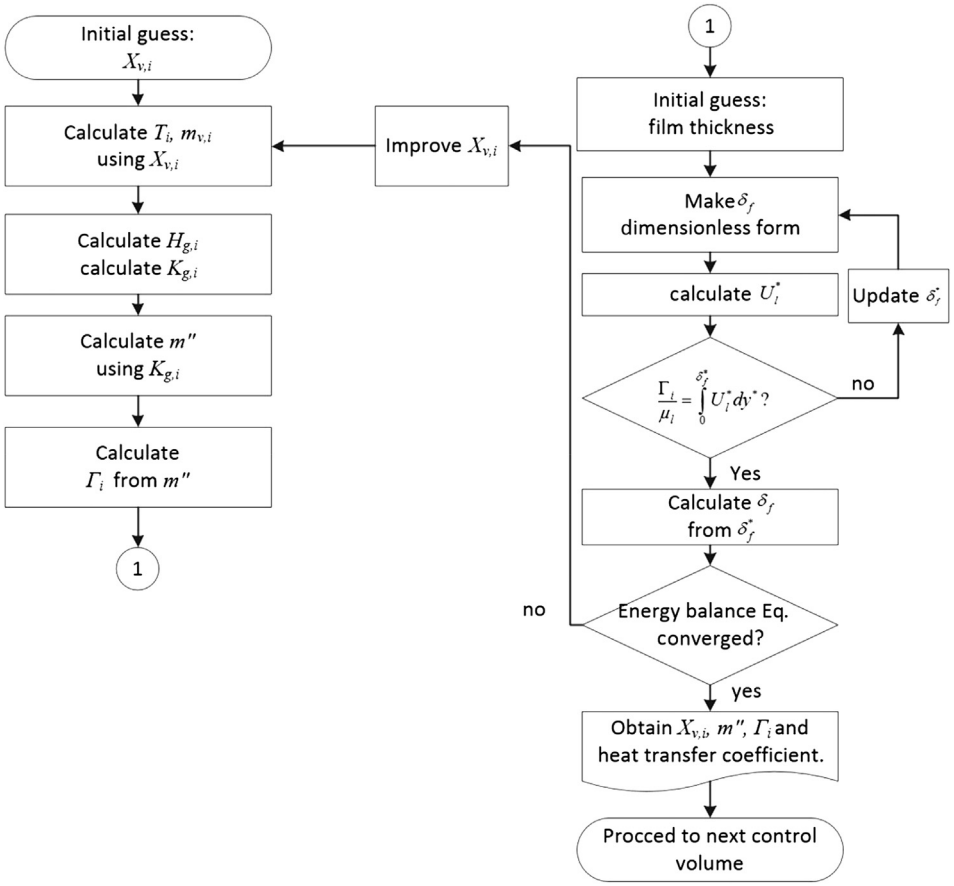

Fig. 8 – Flowchart of the wall condensation model.

In a similar manner, the heat transfer term between the gas and the wall is set to zero and that between the liquid film and the wall is calculated from the film condensation model,

$$q_l'' = k_l \frac{T_{l,1} - T_{l,0}}{\delta y}, \tag{14}$$

where $T_{l,0}$ and $T_{l,1}$ are the wall temperature and the liquid temperature at the first node from the wall in the liquid film subgrid, respectively.

The interfacial area concentration appears in the interfacial transfer terms of the two-fluid model. If the condensation model is activated, considering the topology of the liquid film, the interfacial area concentration is calculated as below,

$$a_i = \frac{A_i}{V_{cell}} = \frac{1}{W}, \tag{15}$$

where W is the width of the cell for two-dimensional quadrilateral mesh.

In the two-fluid model of CUPID, interfacial shear stress is modelled with the relative velocity between two phases,

$$\tau_i = \frac{1}{2} f_i \rho_g |U_g - U_l| (U_g - U_l), \tag{16}$$

where the velocities are phasic averaged ones in a cell. In the filmwise condensation model, it is calculated with the interface velocity as presented in Eq. (4) and for consistency in interfacial momentum exchange evaluation between the liquid film model and the two-fluid model, the interfacial friction factor in the two-fluid model was modified as below,

$$\tau_i = \frac{1}{2} f_i \rho_g |U_g - U_l| (U_g - U_l) = \frac{1}{2} \dot{f} \rho_g |U_g - U_i| (U_g - U_i), \tag{17}$$

$$f_i = \frac{\dot{f} |U_g - U_i| (U_g - U_i)}{|U_g - U_l| (U_g - U_l)}. \tag{18}$$

The phase change rates are:

$$\Gamma_{g,film} = \frac{H_{g,i}(T_g - T_i) + H_{f,i}(T_w - T_i)}{h_g - h_f}, \tag{19}$$

in the film condensation model, and

$$\Gamma_{g,CUPID} = \frac{H_{g,i,CUPID}(T_g - T_s) + H_{f,i,CUPID}(T_f - T_s)}{h_g - h_{f,s}}, \tag{20}$$

in CUPID. It should be noted that the saturation temperature in the two-fluid model, T_s, is calculated using the noncondensable mass fraction and pressure at the cell center, $m_{n,cell}$ and P_{cell}, respectively, but one in the film condensation model, T_i is the saturation temperature estimated with the noncondensable gas mass fraction and the pressure on the interface, $m_{n,i}$ and P_i. Therefore, in order to reproduce the phase change rate evaluated by the film condensation model, the interfacial heat transfer coefficients in CUPID needs to be calculated in the following manner:

$$H_{g,i,CUPID} = \frac{H_{g,i}(T_g - T_i)}{(T_g - T_s)} \frac{(h_g - h_{f,s})}{(h_g - h_f)}, \tag{21}$$

$$H_{f,i,CUPID} = \frac{H_{f,i}(T_f - T_i)}{(T_f - T_s)} \frac{(h_g - h_{f,s})}{(h_g - h_f)}. \tag{22}$$

From these modifications of the wall and interfacial shear stresses and wall and interfacial heat transfers in the two-fluid model, CUPID becomes capable of reproducing the phase change rate, the liquid velocity, and the liquid temperature predicted by the film condensation model.

4. Verification of the implemented model for a large system

Using the improved CUPID code, the wall film condensation in a large system was analyzed and the conceptual problem of Dehbi [2] was selected for verification. Then, the CUPID calculation result was compared with Dehbi's [2] single phase analysis method performed with the wall function approach. Verification was sought by comparing the CUPID calculation results with those of two different approaches. Any discrepancies were then investigated. In this section, Dehbi's [2] conceptual problem is described and the calculation results with the two approaches are compared and discussed.

Dehbi [2] simulated in two dimensions the flow over a hypothetical vertical wall condenser which is 20 m long and 10 m wide. A 2 m distance above and below the condensate wall are allowed for adiabatic flow conditioning. Fig. 9 shows the computational domain of the problem and boundary conditions. A steam-air mixture with 50% steam by mass is assumed to enter the channel from the top with a small velocity of 0.3 m/s. The fluid entrance temperature is set to 405 K and the domain

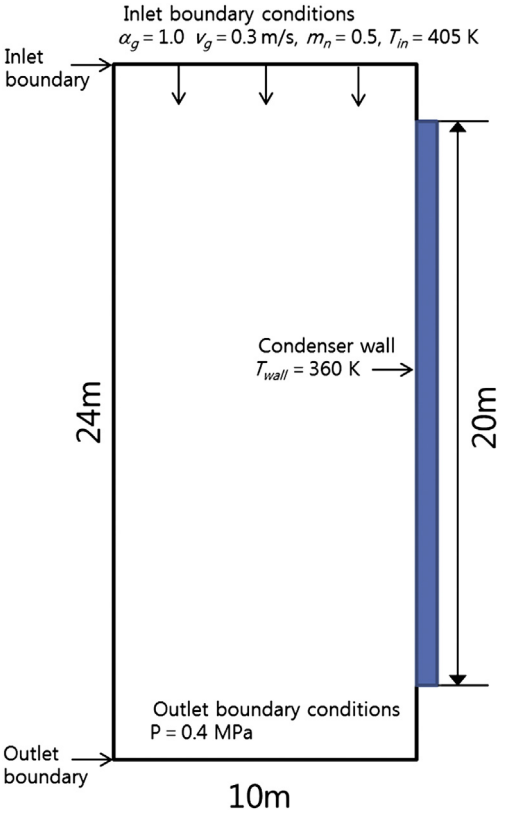

Fig. 9 – Conceptual problem for the film condensation model.

is held at 4.0 bars pressure. The condensate wall temperature is maintained at 360 K. For the calculations, the standard k-ε turbulence model was applied. A mesh convergence test was carried out for the wall heat flux and the liquid film thickness along the condensate wall in three different meshes, 75 × 120, 100 × 180, and 125 × 240 as presented in Fig. 10. Independent of the width of the first cell from the wall, reasonably converged results could be obtained and the maximum heat flux deviation between the calculation results in the finest and the second finest meshes were 5.3% near the condenser top and the averaged difference was 1.2%. Based on this convergence test result, the second finest mesh was selected for the present analysis discussed below. For the chosen mesh, the mean y^+ value of the wall adjacent cells was 52.2.

Figs. 11–14 show the CUPID simulation results conducted with Dehbi's [2] suction correction factor in Eq. (8). As the gas mixture meets the cold wall and the condensation starts, the void fraction near the condensate wall decreases as shown in Fig. 11 and the liquid film thickness consequently increases as shown in Fig. 10B. At the same time, the air mass fraction in the wall adjacent cells increases sharply near the condenser top due to the reduction of the steam mass by the condensation as indicated in Fig. 12. Proceeding downward from the condenser top, due to the increasing density of gas mixture with the air mass fraction, the gas velocity is accelerated as seen in Fig. 13. This results in the increase of turbulent viscosity and accordingly, turbulent diffusivity. It should be noted that the air mass fraction along the condensate wall is determined by the sum between its accumulation due to the wall condensation and the dilution due to the mass diffusion. In the present simulation result of Fig. 12, the air mass fraction increases rapidly as the condensation starts, but makes a turnaround and decreases gradually as the turbulent mass diffusion effect becomes significant. Due to increasing velocity along the condensate wall and the decreasing noncondensable gas mass fraction below a certain elevation, the wall heat flux and the condensation mass flux increase as shown in Fig. 14. On the contrary, if the mass diffusion term is not considered in the two-fluid model, the noncondensable gas is merely accumulated near the condensate wall. Fig. 12 compares the noncondensable gas mass fractions with and without the term. The saturation of the noncondensable gas mass fraction was observed without the term as the mass fraction in the bulk becomes equal to that on the interface and, accordingly, the condensation does not occur any more. Fig. 14 shows the halt of the condensation below 6 m downstream of the condenser top and thereafter, the wall heat transfer is continued by the sensible heat transfer solely between the bulk and the interface. In this way, the mass diffusion term plays a crucial role for an accurate condensation heat transfer analysis in a large system and by the implementation of the present work, CUPID becomes applicable to the condensation analysis with a CFD scale.

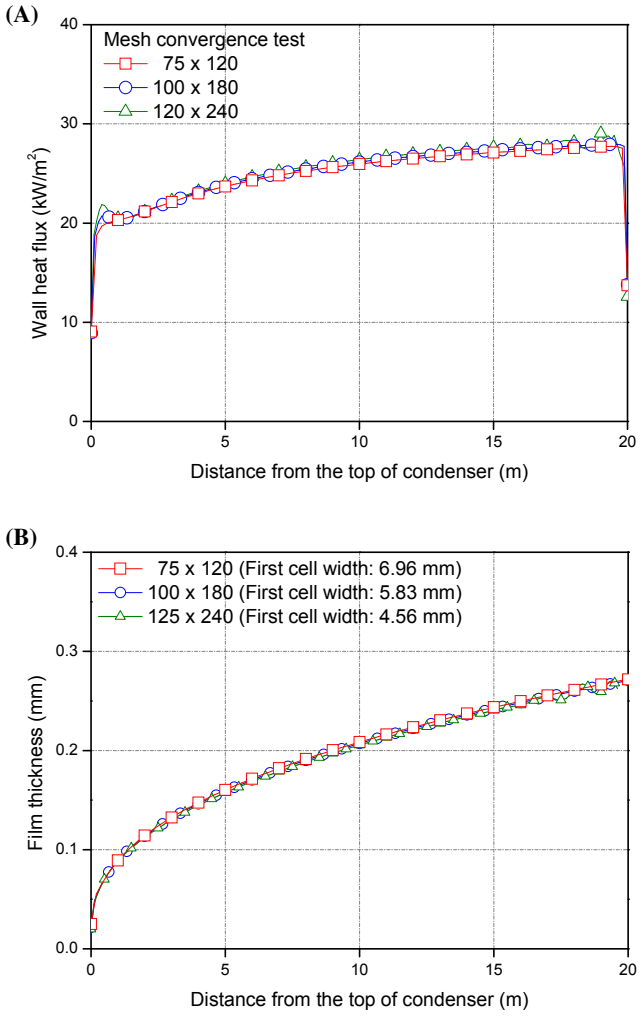

Fig. 10 – Mesh convergence test result. (A) Heat flux. (B) Liquid film thickness.

For verifying the implemented wall condensation model of the CUPID code against the single phase approach, the CUPID calculation result was compared with Dehbi's [2] calculation. Fig. 15 shows the comparison results and three different cases of CUPID calculations were presented; one without suction correction, one with Dehbi's [2] suction correction factor, and one with Bird's suction correction factor. With the application of the suction correction factors, the heat flux curves were shifted up and for all three cases, the increasing trend of the wall heat flux along the condensate wall was reasonably reproduced and comparable results could be obtained. However, the inclination of the heat flux curves were lower in the CUPID simulation and therefore, the heat flux in the upper part of the condensate wall (distance from the condenser top < 5 m) was over-predicted, while that in the lower part was under-predicted when compared with the single-phase approach. This discrepancy can be explained by the relative velocity between the gas and the interface. In the single-phase approach, the wall boundary for the gas is the no-slip wall since the liquid film is neglected. However, in the two-phase approach, the wall boundary for gas is the downward liquid film interface. As indicated in Fig. 13, the relative velocity between the gas and the interface increases in the upper part of the condenser where the gas velocity is rapidly increasing. However, it makes a turnaround and slightly decreases below a certain elevation. The momentum, heat, and mass transfers are significantly influenced by the relative velocity and its decrease may cause the deceleration of the increasing trend of the wall heat flux. However, in the single phase approach, the decreasing trend of the relative velocity cannot be considered

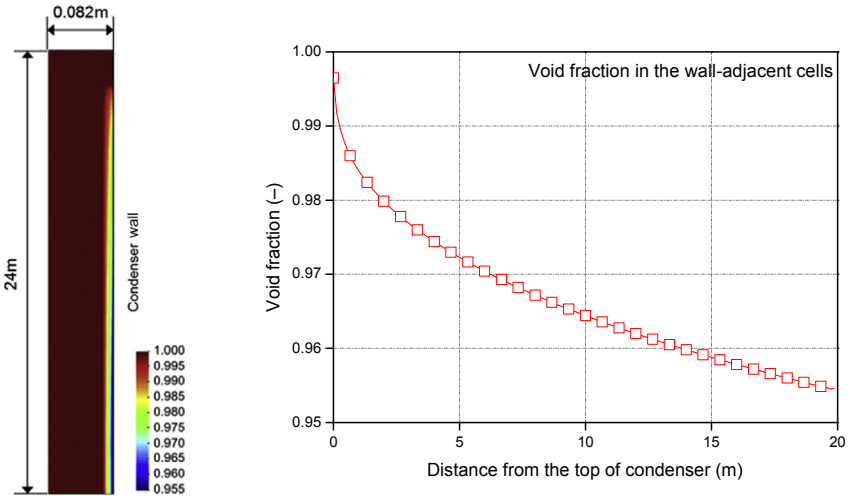

Fig. 11 – Calculation result: void fraction.

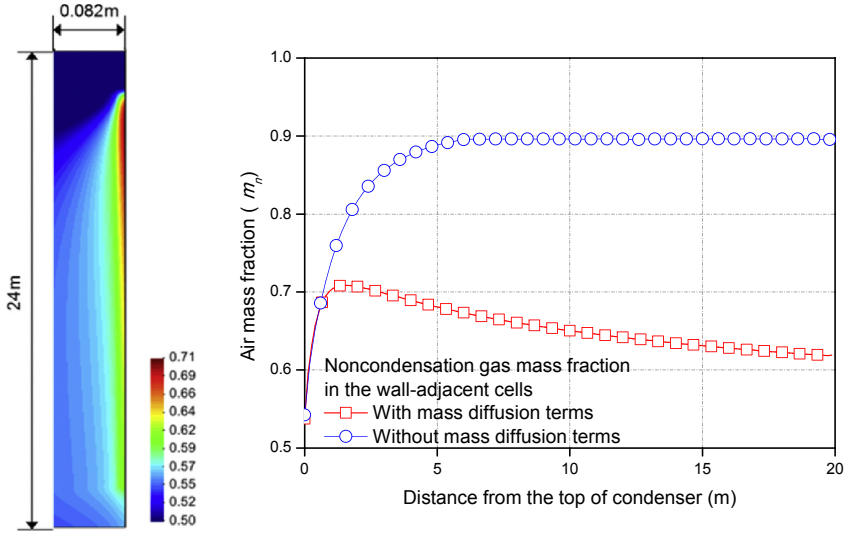

Fig. 12 – Calculation result: noncondensable gas quality.

and the evaluated wall heat flux increases more steeply than in the CUPID result. This difference in the interface velocity treatment can be attributed to the reason of the different inclination of the heat flux, and the effect of the decreasing relative velocity is deemed important when the condensate wall is long so that the liquid film is accelerated sufficiently.

Despite this difference in the interface velocity treatment, it was found from this code-to-code comparison that the implemented wall film condensation model for the two-fluid model produces comparable results to the single-phase approach. However, this model is able to consider the thermal resistance of the liquid film and the influence of the liquid velocity on the gas velocity. This implies that the two-phase flow approach can be applied for more general applications where the thermal resistance of the liquid film cannot be ignored due to a thick liquid film and a low noncondensable gas mass fraction and where the interface velocity has a considerable influence on the heat transfer.

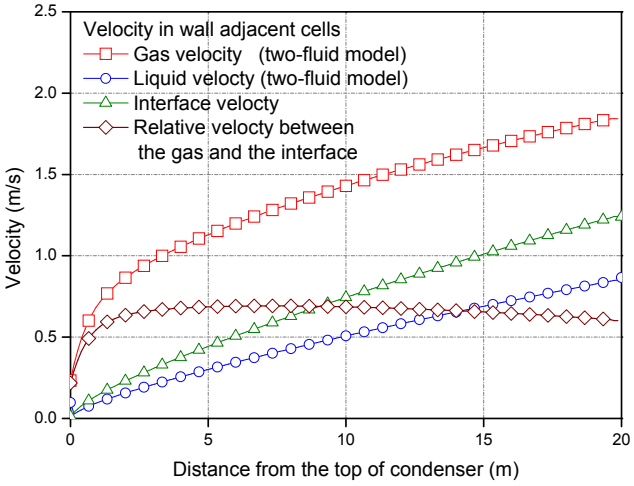

Fig. 13 – Calculation result: velocity.

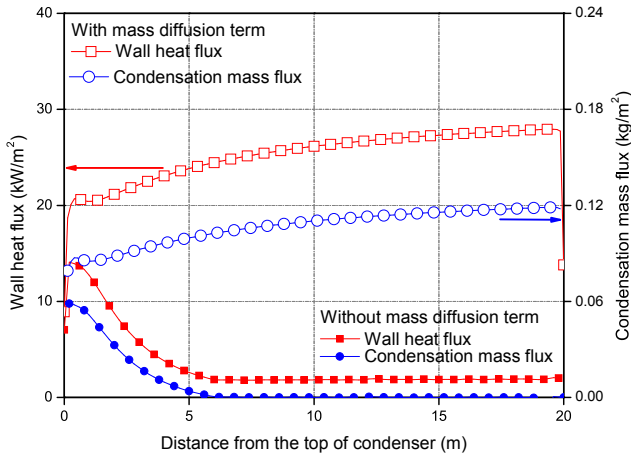

Fig. 14 – Calculation result: wall heat flux and condensation mass flux.

5. Summary and conclusion

In the present study, a two-fluid model CMFD code, CUPID was modified and improved for modeling wall film condensation in the presence of noncondensable gases. At first, the mass diffusion terms were added into the mass and energy equations of the previous version of CUPID in order to predict the noncondensable gas mass fraction on the liquid film-gas interface accurately and the implementation was verified using the code-to-code comparison. Secondly, the liquid film model which can evaluate the velocity and the thickness of the liquid film was implemented and the shear stress terms for the gas and liquid momentum equations were modified. Eventually, a wall film condensation model was proposed, which calculates the condensation rate from the energy conservation equation on the interface. For the evaluation of the heat and mass transfer coefficients, the wall function approach with the heat and mass transfer analogy was applied. The two-fluid model provides the bulk stream information to the wall condensation model at every time step and the model evaluates the magnitudes of relevant terms in the two-fluid model, such as the wall shear stress of liquid, wall heat transfer rate of liquid, interfacial area concentration, interfacial shear stress, interfacial heat transfer coefficients for gas and liquid, etc. This implemented model was verified by solving Dehbi's [2] conceptual problem and comparing the results between single-phase and two-phase approaches. A fairly good agreement was obtained between the present approach and that of Dehbi [2] even though a discrepancy in the inclination of the condensation heat flux was observed due to the difference in the treatment of the interface velocity.

In the future, further validation will be performed with this film condensation model for the two-fluid model against various experimental databases, not only for the vertical flat plate but also for tube geometry in order to extend its capability to a passive containment cooling system where a film condensation occurs on a tube bundle.

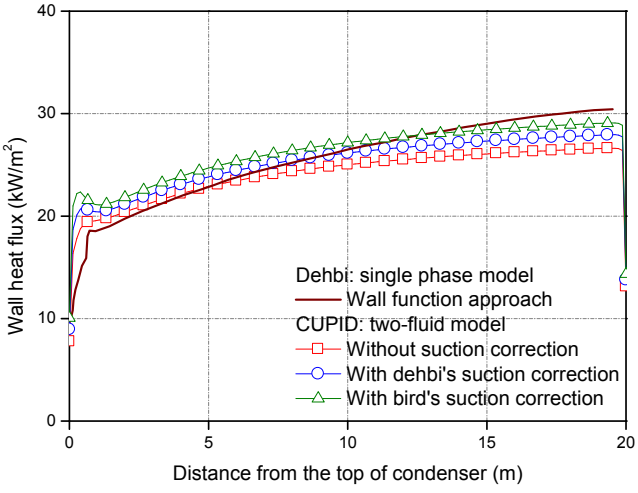

Fig. 15 – Comparison between CUPID and Dehbi's calculation results.

Conflicts of interest

The authors have no conflicts of interest.

Acknowledgments

This work was supported by the Korea Radiation Safety Foundation (KORSAFE) grant funded by the Korean Government (NSSC) (1305011) (Nuclear Safety Research Center Program: 1305011).

Nomenclature

a	area concentration (1/m)
A	cell area (m^2)
D	effective diffusivity (m^2/s)
e	internal energy (J/kg)
E	eddy diffusivity (m^2/s)
f	fanning friction factor
g	gravity acceleration (m/s^2)
h	enthalpy (J/kg)
H	heat transfer coefficient (W/m^2K)
k	thermal conductivity (W/mK)
K	mass transfer coefficient (kg/m^2s)
m	mass fraction
m''	condensation mass flux (kg/m^2s)
M	molecular weight (kg/mol)
$\dot{M}$	momentum exchange (kg/m^2s^2)
P	pressure (Pa)
Pr	Prandtl number
q''	heat flux (W/m^2)
Sc	Schmidt number
T	temperature (K)
U	velocity (m/s)
V	Volume (m^3)

W	width of the cell (m)
X	mole fraction

Greek symbols

α	void fraction
Γ	mass flow rate (kg/ms)
δ	thickness (m)
θ	angle
μ	dynamic viscosity (kg/ms)
ρ	density (kg/m^3)
υ	kinematic viscosity (m^2/s)
τ	shear stress (Pa)

Subscript

b	bulk stream
f	film
film	film condensation model
g	gas mixture
i	interface
l	liquid
n	noncondensable gas
s	saturated
v	vapor
w	wall

REFERENCES

[1] A. Dehbi, F. Janasz, B. Bell, Prediction of steam condensation in the presence of noncondensable gases using a CFD-based approach, Nucl. Eng. Des. 258 (2013) 199–210.

[2] A. Dehbi, On the adequacy of wall functions to predict condensation rates from steam-noncondensable gas mixtures, Nucl. Eng. Des. 265 (2013) 25–34.

[3] W. Ambrosini, N. Forgione, F. Merli, F. Oriolo, S. Paci, I. Kljenak, P. Kostka, L. Vyskocil, J.R. Travis, J. Lehmkuhl, S. Kelm, Y.-S. Chin, M. Bucci, Lesson learned from the SARNET wall condensation benchmarks, Ann. Nucl. Energy 74 (2014) 153–164.

[4] W. Ambrosini, N. Forgione, F. Oriolo, C. Dannöhl, H.J. Konle, Experiments and CFD analyses on condensation heat transfer on a flat plate in a square cross section channel, 11th International Topic Meeting in Nuclear Reactor Thermal-Hydraulics (NURETH-11), vol. CD-ROM. Popes' Palace Conference Center, pp. 1–18, Avigon, France, October 2nd–6th, 2005.

[5] J.M. Martín-Valdepeñas, M.A. Jiménez, F. Martín-Fuertes, J.A. Fernández, Benítez, Comparison of film condensation models in presence of non-condensable gases implemented in a CFD Code, Heat Mass. Transf. 41 (2005) 961–976.

[6] L. Vyskocil, J. Schmid, J. Macek, CFD simulation of air-steam flow with condensation, Nucl. Eng. Design. 279 (2014) 147–157.

[7] G. Zschaeck, T. Frank, A.D. Burns, CFD modeling and validation of wall condensation in the presence of non-condensable gases, Nucl. Eng. Des. 279 (2014) 137–146.

[8] OECD/NEA SETH-2 Project: OECD/SETH-2 Project PANDA and MISTRA Experiments–Investigation of Key Issues for the Simulation of Thermal-hydraulic Conditions in Water Reactor Containments final summary report, NEA/CSNI/R, 2012, p. 5.

[9] S.Z. Kuhn, Investigation of heat transfer from condensing steam-gas mixtures and turbulent films flowing downward inside a vertical tube, Ph.D. Thesis, University of California, Berkeley (, 1995.

[10] X. Cheng, P. Bazin, P. Cornet, D. Hittner, J.D. Jackson, J. Lopez Jimenez, A. Naviglio, F. Oriolo, H. Petzold, Experimental data base for containment thermal-hydraulic analysis, Nucl. Eng. Des. 204 (2001) 267–284.

[11] J. Malet, E. Porcheron, J. Vendel, OECD International Standard Problem ISP-47 on containment thermal-hydraulics-Conclusions of the TOSQAN part, Nucl. Eng. Des. 240 (2010) 3209–3220.

[12] H. Uchida, et al., Evaluation of post-incident cooling systems of light-water power reactors, in: Proceedings of the Third International Conference on Peaceful Uses of Atomic Energy, Geneva, August 27th–September 9th, Vol. 13, 1965, pp. 93–104. United Nations, New York.

[13] T. Tagami, Interim Report on Safety Assessments and Facilities Establishment Project for June 1965, No. 1, Japanese Atomic Energy Research Agency, 1965. unpublished data.

[14] A. Dehbi, M. Golay, M.S. Kazimi, Condensation experiments in steam–air and steam–air–helium mixtures under turbulent natural convection, in: National Heat Transfer Conference, AIChE, Minneapolis, 1991, pp. 19–28.

[15] M.L. Corradini, Turbulent condensation on a cold wall in the presence of a noncondensable gas, Nucl. Technol. 64 (1984) 186–195.

[16] S. Mimouni, J.-S. Lamy, J. Lavielle, S. Guieu, M. Martin, Modeling of sprays in containment applications with a CMFD code, Nucl. Eng. Des. 240 (2010) 2260–2270.

[17] S. Mimouni, A. Foissac, J. Lavielle, CFD modelling of wall steam condensation by a two-phase approach, Nucl. Eng. Des. 241 (2011) 4445–4455.

[18] CD adapco, CD-adapco USER GUIDE STAR-CCM+ Version 8.06, CD-adapco, 2013.

[19] H.Y. Yoon, et al., CUPID Code Manual Vol. 1: Mathematical Models and Solution Methods, Korea Atomic Energy Research Institute, KAERI/TR-4403/2011, 2011.

[20] J.-J. Jeong, H.-Y. Yoon, I.-K. Park, H.-K. Cho, H.-D. Lee, Development and preliminary assessment of a three-dimensional thermal hydraulics code, CUPID, Nucl. Eng. Technol. 42 (2010) 279–296.

[21] H.Y. Yoon, J.R. Lee, H. Kim, I.K. Park, C.-H. Song, H.K. Cho, J.J. Jeong, Recent improvements in the cupid code for a multi-dimensional two-phase flow analysis of nuclear reactor components, Nucl. Eng. Technol. 46 (2014) 655–666.

[22] T. Fuji, Y. Kato, K. Mihara, Expressions of transport and thermodynamic properties of air, steam and water, University of Kyushu, Rept. 66 (1977) 81–95.

[23] M. Jischa, H.B. Rieke, About the prediction of turbulent prandtl and schmidt numbers from modeled transport equations, Int. J. Heat Mass Transfer 22 (1979) 1547–1555.

[24] S.M. Ghiaasiaan, Two-phase Flow, Boiling and Condensation, Cambridge University Press, New York, 2008.

[25] F.M. White, Fluid Mechanics, seventh ed., Mc GRAW-HILL, Singapore, 2010.

[26] I. Mudawar, M.A. El-Marsi, Momentum and heat transfer across freely-falling turbulent liquid films, Int. J. Heat Mass Transfer 12 (1986) 771–790.

[27] D. Naylor, J. Friedman, Model of film condensation on a vertical plate with noncondensing gas, J. Thermophys. Heat Transfer 24 (2010) 501–505.

[28] B. Koncar, M. Borut, Wall function approach for boiling two-phase flow, Nucl. Eng. Des. 240 (2010) 3910–3918.

[29] E. Kerpper, B. Končar, Y. Egorov, CFD modeling of subcooled boiling–concept, validation and application to fuel assembly design, Nucl. Eng. Des. 237 (2007) 716–731.

[30] B.J. Yoon, A. Splawski, S. Lo, C.-H. Song, Prediction of a subcooled boiling flow with advanced two-phase flow models, Nucl. Eng. Des. 251 (2012) 351–359.